Neuron
NeuroResource

Imaging Neural Activity Using *Thy1*-GCaMP Transgenic Mice

Qian Chen,[1] Joseph Cichon,[3,10] Wenting Wang,[1,10] Li Qiu,[4] Seok-Jin R. Lee,[4] Nolan R. Campbell,[1] Nicholas DeStefino,[6] Michael J. Goard,[2] Zhanyan Fu,[1,5] Ryohei Yasuda,[4] Loren L. Looger,[7] Benjamin R. Arenkiel,[8] Wen-Biao Gan,[3] and Guoping Feng[1,9,*]

[1]McGovern Institute for Brain Research, Department of Brain and Cognitive Sciences
[2]Picower Institute for Learning and Memory, Department of Brain and Cognitive Sciences
Massachusetts Institute of Technology, Cambridge, MA 02139, USA
[3]Molecular Neurobiology Program, Skirball Institute, Department of Physiology and Neuroscience, New York University School of Medicine, New York, NY 10016, USA
[4]Department of Neurobiology
[5]Department of Psychiatry and Behavioral Science
Duke University Medical Center, Durham, NC 27710, USA
[6]MD-PhD Program, Harvard Medical School, Boston, MA 02115, USA
[7]Howard Hughes Medical Institute, Janelia Farm Research Campus, Ashburn, VA 20147, USA
[8]Department of Molecular and Human Genetics, Baylor College of Medicine, Houston, TX 77030, USA
[9]Stanley Center for Psychiatric Research, Broad Institute, Cambridge, MA 02142, USA
[10]These authors contributed equally to this work
*Correspondence: fengg@mit.edu
http://dx.doi.org/10.1016/j.neuron.2012.07.011

SUMMARY

The ability to chronically monitor neuronal activity in the living brain is essential for understanding the organization and function of the nervous system. The genetically encoded green fluorescent protein-based calcium sensor GCaMP provides a powerful tool for detecting calcium transients in neuronal somata, processes, and synapses that are triggered by neuronal activities. Here we report the generation and characterization of transgenic mice that express improved GCaMPs in various neuronal subpopulations under the control of the *Thy1* promoter. In vitro and in vivo studies show that calcium transients induced by spontaneous and stimulus-evoked neuronal activities can be readily detected at the level of individual cells and synapses in acute brain slices, as well as chronically in awake, behaving animals. These GCaMP transgenic mice allow investigation of activity patterns in defined neuronal populations in the living brain and will greatly facilitate dissecting complex structural and functional relationships of neural networks.

INTRODUCTION

Monitoring neuronal activity is critical for our understanding of both normal brain function and pathological mechanisms of brain disorders. Because neuronal activity is tightly coupled to intracellular calcium dynamics, calcium imaging has proven invaluable for probing the activities of neuronal somata, processes, and synapses both in vitro and in vivo (Andermann et al., 2011; Chen et al., 2011; Kerr and Denk, 2008; Yasuda et al., 2004). Compared to multielectrode recording approaches, calcium imaging has the advantages of detecting activity in large or disperse populations of neurons simultaneously over extended periods of time with little or no mechanical disturbance to brain tissues.

Synthetic calcium dyes have been widely used to monitor intracellular calcium dynamics in cultured neurons, brain slices, as well as in the intact brain (Chen et al., 2011; Dombeck et al., 2007; Kerr and Denk, 2008; Marshel et al., 2011; Rothschild et al., 2010; Yasuda et al., 2004). However, loading calcium dyes into specific neuronal populations is technically challenging. It is difficult, if not impossible, to image activities of the same neuronal populations repeatedly over extended periods of time. Genetically encoded calcium indicators (GECIs) overcome these difficulties, permitting chronic imaging of calcium dynamics within specific cell types. GECIs are composed solely of translated amino acids and do not require the addition of synthetic compounds or cofactors. They can be targeted to specific cell types or subcellular compartments when used in combination with cell type-specific promoters or cellular targeting sequences. In addition, GECIs can be delivered and expressed in brain tissues via viral vectors, in utero electroporation, or through transgenic techniques (Hasan et al., 2004; Mao et al., 2008; Wallace et al., 2008; Yamada et al., 2011). Importantly, recently developed GECIs are capable of detecting calcium dynamics at the sensitivity level close to that of synthetic calcium dyes (Hendel et al., 2008; Pologruto et al., 2004).

At least one class of green fluorescent protein (GFP)-based GECIs, the GCaMP family, has been effective for detecting calcium dynamics induced by neuronal activity in multiple model organisms (Muto et al., 2011; Reiff et al., 2005; Tian et al., 2009; Warp et al., 2012). Recently, a new generation of GCaMPs (e.g., GCaMP3) has been successfully used to monitor neuronal

activity in rodents using viral approaches (Borghuis et al., 2011; Dombeck et al., 2010; Mittmann et al., 2011; Osakada et al., 2011; Tian et al., 2009). Here we report the generation and characterization of new transgenic mouse lines that express the improved GCaMP2.2c and GCaMP3 indicators (Tian et al., 2009) in subsets of excitatory neurons in the mouse brain using the *Thy1* promoter. We demonstrate long-term, stable expression of GCaMPs in subpopulations of neurons with no apparent toxicity. Both GCaMP2.2c and GCaMP3 show strong and sensitive changes in fluorescence upon neuronal stimulation. We further demonstrate the broad utility of *Thy1*-GCaMP2.2c and *Thy1*-GCaMP3 transgenic mice in reporting neuronal activity in vitro and in vivo.

RESULTS

Generation of *Thy1*-GCaMP2.2c and *Thy1*-GCaMP3 Transgenic Mice

To generate GCaMP transgenic mice, we utilized the previously described GCaMP3 and a further modified GCaMP2.2b (Tian et al., 2009). Previous studies suggested that the N-terminal arginine located immediately after the initiator methionine of GCaMP2.0 destabilizes the protein, and changing the serine at 118 to cysteine could improve brightness and sensor response (Tian et al., 2009). Thus, we changed the second arginine in GCaMP2.0 to valine to increase its stability according to the N-terminal rule of protein degradation (Varshavsky, 2011) and changed the serine at 118 to cysteine as in GCaMP2.2b to create GCaMP2.2c. The domain structure and specific mutations of GCaMP2.2c and GCaMP3 are summarized in Figure S1A, available online.

Two important properties to consider when evaluating GECIs are basal levels of fluorescence and stimulation-induced changes in fluorescence ($\Delta F/F$). To assess these properties for GCaMP2.2c and GCaMP3, we coexpressed GCaMPs and the red fluorescence protein tdTomato in the same construct using the 2A peptide (P2A) sequence (Szymczak et al., 2004) in HEK293 cells. To normalize for transfection efficiency, we used the fluorescence intensity ratio of GCaMPs/tdTomato. We found that GCaMP3 showed significantly higher basal fluorescence compared to GCaMP2.2c and GCaMP2.0, whereas there was no significant difference between the basal fluorescence of GCaMP2.0 and GCaMP2.2c (Figures S1B and S1C). In addition, we found that fluorescence intensity changes elicited by 100 μM ATP are ~1.9-fold (1.9 ± 0.1, n = 56) and ~3.2-fold (3.2 ± 0.3, n = 61) higher in cells expressing GCaMP2.2c and GCaMP3 than in cells expressing GCaMP2.0, respectively (Figure S1D).

The studies above indicate that GCaMP2.2c has a low basal fluorescence with a modest fluorescence change in response to stimulation, whereas GCaMP3 shows higher basal fluorescence and a more robust change in fluorescence after stimulation. Because GCaMP (and any GECI) binds calcium, there is a risk of neuronal toxicity associated with calcium binding and expression level. To increase the chances of finding lines with both strong signal and low toxicity, we generated both GCaMP2.2c and GCaMP3 transgenic lines.

To generate GCaMP transgenic mice, we used the well-characterized *Thy1* promoter to express GCaMPs in neurons.

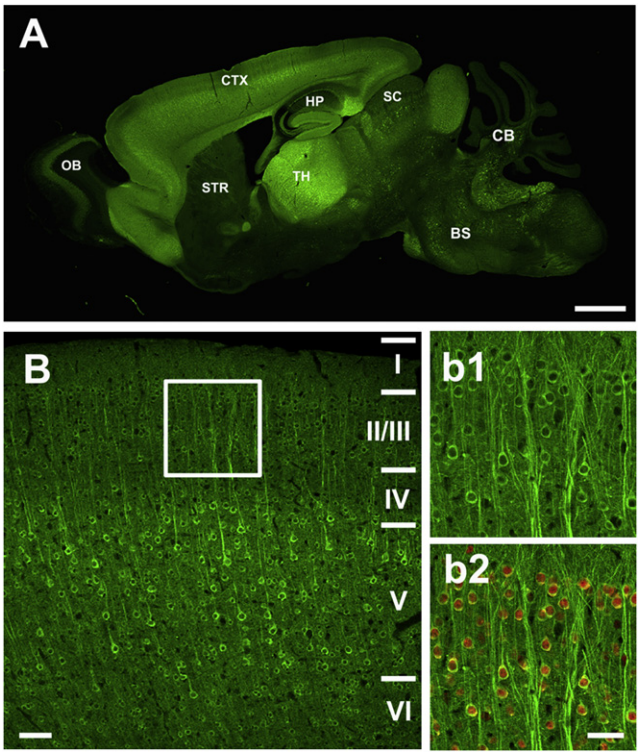

Figure 1. Expression Patterns of *Thy1*-GCaMP3 Transgenic Mice

(A) A sagittal section of brain from a *Thy1*-GCaMP3 mouse. GCaMP3 is highly expressed in the cortex, hippocampus, thalamus, superior colliculus, and mossy fiber in the cerebellum and various nuclei in the brain stem.

(B) Confocal images showing the expression in motor cortex (M1) of *Thy1*-GCaMP3 mouse brains. The insets (b1 and b2) show a higher-magnification view of layer II/III neurons in the cortex (boxed area). GCaMP3 is expressed in most layer II/III neurons. In (b1) and (b2), the same section was costained with an antibody against the neuronal marker NeuN (red) showing the localization of GCaMP in the cytoplasm of neurons. OB, olfactory bulb; CTX, cortex; HP, hippocampus; STR, striatum; TH, thalamus; SC, superior colliculus; CB, cerebellum; BS, brain stem. I, II, III, IV, V, and VI refer to cortical layers. Scale bars represent 1 mm in (A) and 50 μm in (B) and (Bb2).

We generated eight founder lines of GCaMP2.2c and six founder lines of GCaMP3. Our previous studies have shown that the *Thy1* promoter predominantly drives transgene expression in projection neurons in the CNS. Due to strong transgenic position-effect variegation, a *Thy1*-driven transgene is often stochastically and differentially expressed in subsets of neurons in different transgenic lines (Feng et al., 2000; Young et al., 2008). Consistent with these findings, we found that all founder lines differed in levels and patterns of expression. For further characterization, we focused on *Thy1*-GCaMP2.2c line 8 and *Thy1*-GCaMP3 line 6 because these lines had the highest levels of transgene expression. Both lines of mice are born at the expected Mendelian rate and are healthy with no apparent histological or behavioral abnormality. GCaMP2.2c and GCaMP3 expression in these lines was widespread in the CNS including cortex, hippocampus, thalamus, cerebellum, superior colliculus, amygdala, brain stem, retina, and spinal cord (Figures 1A, 1B, and 2; Figure S2). However, some notable differences in expression

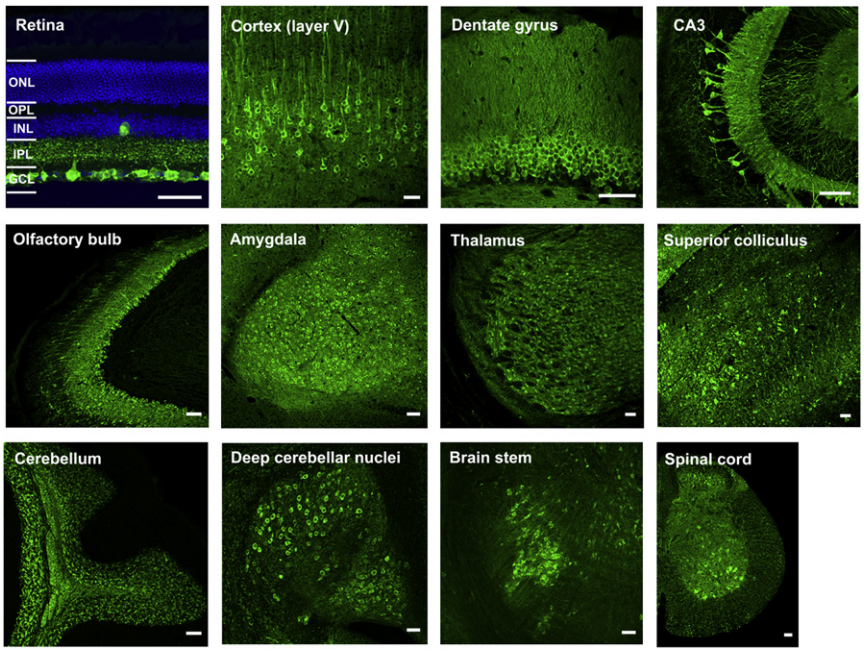

Figure 2. GCaMP Fluorescence in *Thy1*-GCaMP3 Transgenic Mice Showing Labeling of Subsets of Neurons in Different Brain Areas

Green, GCaMP fluorescence; blue, DAPI staining. GCL, ganglion cell layer; IPL, inner plexiform layer; INL, inner nuclear layer; OPL, outer plexiform layer; ONL, outer nuclear layer. Scale bars represent 50 μm.

between the two lines were observed. For example, although both lines have expression in layer V neurons of the cortex, expression in layer II/III is more widespread in the *Thy1*-GCaMP3 line (Figures 1B, 1Bb1, and 1Bb2) compared to the *Thy1*-GCaMP2.2c line (Figures S2B, S2Bb1, and S2Bb2). In addition, *Thy1*-GCaMP3 mice, but not *Thy1*-GCaMP2.2c mice, showed high expression in olfactory bulb (Figures 1A and 2). At the single cell level, both GCaMP2.2c and GCaMP3 were homogeneously distributed in the cytoplasm without nuclear localization (Figures 1B, 1Bb1, and 1Bb2; Figures S2B, S2Bb1, and S2Bb2). We further examined the effect of long-term GCaMP expression in both GCaMP transgenic lines. We did not find any cells with GCaMP-filled nuclei from 2- to 12-month-old animals in either *Thy1*-GCaMP2.2c or *Thy1*-GCaMP3 lines (Figure S3A). There were very few cells expressing GCaMP in layer II/III before 4 months in *Thy1*-GCaMP2.2c lines. The expression of GCaMP in *Thy1*-GCaMP3 lines was widespread in layer II/III and layer V from 2 to 12 months (Figure S3B). The brightness of GCaMP in both lines increased from 2 to 4 months and was stable after 4 months of age (Figure S3C).

In Vitro Characterization of *Thy1*-GCaMP Mice

To determine GCaMP reporter function in transgenic brain tissues, we used laser-scanning confocal microscopy to monitor Ca^{2+} responses in acute brain slices from 1-month-old *Thy1*-GCaMP2.2c and *Thy1*-GCaMP3 mice. First, we noted that the improved properties of GCaMP2.2c and GCaMP3 allowed for robust calcium imaging of spontaneous activity in layer V neurons of the cortex and in neurons from the CA1 and the dentate gyrus of hippocampus (Movies S1 and S2). To test whether these spontaneous fluorescence changes were associated with neuronal activities, we performed cell-attached recording of spontaneous spike activity and imaged fluorescence changes simultaneously in the hippocampal pyramidal cells. As expected, the fluorescence changes were well correlated with the spontaneous spiking activities in these neurons (Figure S4).

Next, we measured action potential (AP)-triggered fluorescence responses of GCaMP2.2c and GCaMP3. We made whole-cell recordings from GCaMP-expressing hippocampal dentate granular cells and evoked APs by brief current injections (3–5 nA, 2 ms). Single AP evoked Ca^{2+} transients with average $\Delta F/F$ amplitudes of 21.6% ± 1.4% and 25.8% ± 2.0% (n = 9 cells) in *Thy1*-GCaMP2.2c and *Thy1*-GCaMP3 acute slices, respectively. Moreover, the average $\Delta F/F$ and the number of APs were well correlated. The average $\Delta F/F$ of GCaMP2.2c (n = 9 cells) was 65.0% ± 10.5%, 96.6% ± 13.0%, 126.1% ± 15.2%, 146.6% ± 16.8%, 261.4% ± 23.3%, and 308.9% ± 24.2% for 3, 5, 7, 9, 20, and 40 APs, respectively. Similarly, the average $\Delta F/F$ of GCaMP3 (n = 9 cells) was 69.8% ± 14.5%, 119.5% ± 16.1%, 159.8% ± 19.9%, 200.2% ± 22.1%, 343.5% ± 31.2%, and 396.6% ± 28.2% for 3, 5, 7, 9, 20, and 40 APs, respectively (Figures 3A–3D). The signal-to-noise ratio (SNR) of GCaMP2.2c and GCaMP3 was 7.5 ± 0.4 versus 11.9 ± 0.9, 32.7 ± 6.0 versus 46.9 ± 5.5, and 110.5 ± 15.4 versus 148.1 ± 13.6 for 1, 5, and 40 APs, respectively (Figure 3E). The rise times of fluorescence changes range from 214.1 ms to 374.1 ms for both GCaMP2.2c and GCaMP3. Decay times were between 0.9 s and 1.9 s for GCaMP2.2c and 1.4 s and 2.6 s for GCaMP3 (Figures 3F and 3G). Finally, we tested *Thy1*-GCaMP2.2c and *Thy1*-GCaMP3 for the ability to image calcium transients in populations of neuronal somata. For this, we treated acute brain slices from *Thy1*-GCaMP2.2c and *Thy1*-GCaMP3 mice with a high-potassium bath solution. We found that depolarization with high potassium (10 mM and 30 mM KCl) induced dramatic fluorescence changes in dentate granular neurons of the hippocampus in both transgenic lines (Movie S3). The averaged $\Delta F/F$ of GCaMP3 was higher than GCaMP2.2c (217.9% ± 9.4% versus 136.3% ± 6.1% with 10 mM KCl and 310.1% ± 11.8% versus 186.5% ± 10.2% with 30 mM KCl) (Figures S5A and S5B). Thus, at the single cell or population levels, both GCaMP2.2c and GCaMP3 robustly detect spontaneous and evoked responses in vitro in acute brain slice preparations.

In Vivo Ca^{2+} Imaging of Apical Dendrites of Layer V Pyramidal Neurons in the Motor Cortex

To evaluate GCaMP expression in the intact brain, we performed transcranial two-photon imaging of the motor cortex of adult

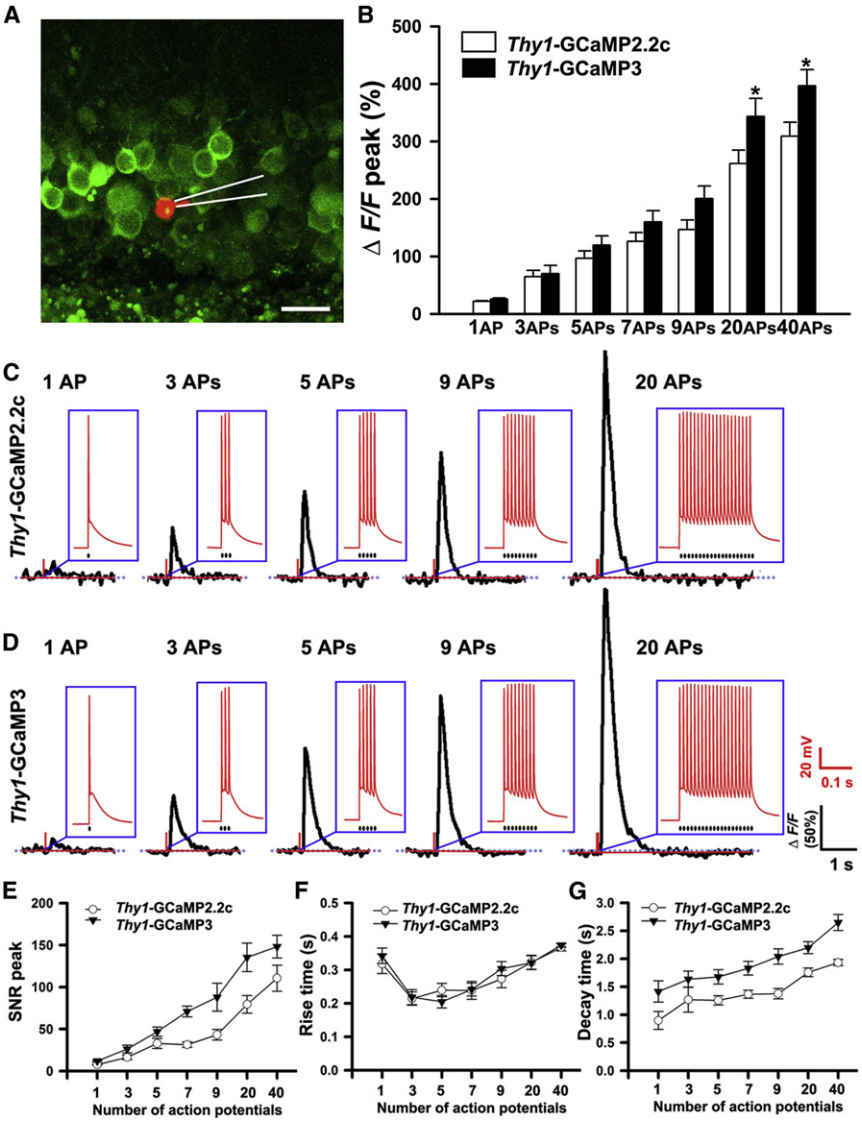

Figure 3. Action Potential-Evoked Response of GCaMP2.2c and GCaMP3 in Hippocampal Granular Cells of *Thy1*-GCaMP Transgenic Mice

(A) A granular cell patched with internal solution containing 100 μM Alexa Fluor 555 is shown in red. The recording pipette is indicated with white lines.

(B) Fluorescence changes of GCaMP2.2c and GCaMP3 to different numbers of action potentials evoked at 83 Hz (n = 9 cells).

(C and D) Representative Δ*F*/*F* traces to different numbers of action potentials across cells from *Thy1*-GCaMP2.2c (C) and *Thy1*-GCaMP3 (D) transgenic mice. The insets show the evoked action potentials from each cell.

(E) Signal-to-noise ratio of GCaMP2.2c and GCaMP3 to different numbers of action potentials evoked at 83 Hz (n = 9 cells).

(F and G) The means of rise time (F) and decay time (G) of fluorescence responses corresponding to the number of stimulating action potentials (n = 9 cells).

Data are presented as mean ± SEM. *p < 0.05. Scale bar represents 50 μm in (A).

Thy1-GCaMP2.2c and *Thy1*-GCaMP3 mice. Under in vivo imaging conditions in both transgenic lines, GCaMP expression was clearly perimembrane and was never detected in the nucleus (Figures 4A–4F and Movies S4 and S5). The baseline fluorescence intensity of GCaMP was similar in both lines in 5-month-old animals (Figure 4G). In *Thy1*-GCaMP2.2c mice, densely packed yet resolvable individual apical tuft dendrites were clearly visible in superficial cortical layers (Figures 4A and 4B). In comparison, the density of labeled dendrites was substantially higher in *Thy1*-GCaMP3 animals, making individual dendritic imaging difficult (Figures 4D and 4E). Consistent with the expression data from fixed brain slices (Figure S2B), *Thy1*-GCaMP2.2c mice had mainly layer V neuron labeling with very rare layer II/III neuron labeling (Figures 4C and 4H), whereas GCaMP3 was expressed in layer V neurons as well as in the majority of layer II/III neurons (Figures 4F and 4H). Therefore, unlike *Thy1*-GCaMP3 mice, *Thy1*-GCaMP2.2c mice offer an opportunity to image the activity of apical dendrites and spines of layer V pyramidal neurons in the cortex.

We next investigated whether *Thy1*-GCaMP2.2c and *Thy1*-GCaMP3 mice could report neuronal activity responses in the intact brain. Since individual dendrites are clearly resolvable in *Thy1*-GCaMP2.2c mice compared to *Thy1*-GCaMP3 mice, we tested whether calcium transients could be detected in the apical dendrites of layer V neurons of *Thy1*-GCaMP2.2c mice using two-photon microscopy in the primary motor cortex (M1). In awake, head-fixed animals, we observed numerous dendritic Ca^{2+} transients with large amplitudes (Figures 5A and 5C). These dendritic Ca^{2+} transients typically lasted several hundreds of milliseconds with a Δ*F*/*F* ranging from ~50% up to 200% (Figure 5B). The duration and amplitude of these dendritic calcium transients are comparable to dendritic calcium spikes observed in vitro (Larkum et al., 2009). In contrast, we rarely observed such robust Ca^{2+} transients in dendritic branches in anesthetized mice (Figure 5C). Furthermore, in the awake state, large elevations of calcium influx were readily detected not only in the entire dendritic shafts but also in their associated dendritic spines (Figures 5A and 5D and Movie S6). In both anesthetized and awake mice, we were able to detect transient calcium elevations within single dendritic spines over tens of milliseconds (Figure 5E). Thus, *Thy1*-GCaMP2.2c mice provide a means for investigating calcium transients over time in dendritic spines, as well as dendritic branches in layer V pyramidal neurons.

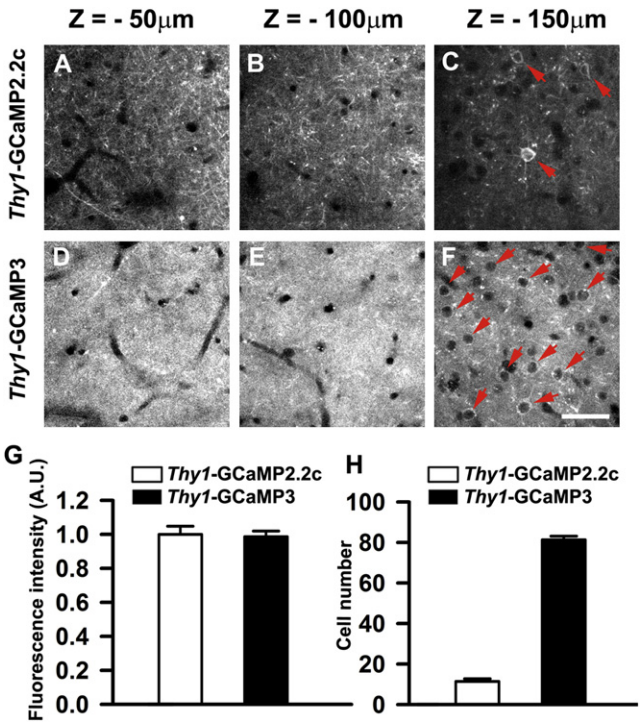

Figure 4. In Vivo Two-Photon Imaging of GCaMP2.2c- and GCaMP3-Expressing Neocortical Neurons

In vivo two-photon images of GCaMP-expressing neurons in the motor cortex of 5-month-old *Thy1*-GCaMP2.2c (A–C) and *Thy1*-GCaMP3 (D–F) mice. The depth below the pial surface is shown above each panel. In *Thy1*-GCaMP2.2c mice, densely packed yet resolvable individual dendrites were clearly visible in the superficial layers (A and B), whereas the density of labeled dendrites was much higher in *Thy1*-GCaMP3 animals (D and E). *Thy1*-GCaMP2.2c mice had few layer II/III neurons labeled (C), whereas GCaMP3 was expressed in almost all layer II/III neurons (F). Red arrows mark individual layer II/III neurons. See also Movies S4 and S5.

(G) Quantification of brightness of neuronal somata from *Thy1*-GCaMP2.2c and *Thy1*-GCaMP3 transgenic mice (~150–160 μm below the pial surface, n = 75 from 3 mice).

(H) Quantification of neuron number in 250 × 250 μm area from *Thy1*-GCaMP2.2c and *Thy1*-GCaMP3 transgenic mice (~150–160 μm below the pial surface, n = 10 from 3 mice). A.U., arbitrary units. Data are presented as mean ± SEM. Scale bar represents 50 μm.

In Vivo Ca^{2+} Imaging of Somatic Activity in the Motor Cortex

Next, we examined whether calcium transients could also be detected in individual somata of *Thy1*-GCaMP mice. We first tested whether we could detect GCaMP responses in the soma of neurons in layer II/III of the motor cortex in anesthetized animals. In *Thy1*-GCaMP2.2c mice, we observed GCaMP-expressing neurons but could not detect activated cells within an imaging window of 250 × 250 μm during a 10 min recording period. In contrast, in *Thy1*-GCaMP3 mice, we observed 9.3 ± 0.5 cells (n = 4 areas from 3 mice) using the same imaging conditions (Figures 6A and 6B). Differences between *Thy1*-GCaMP2.2c and *Thy1*-GCaMP3 mice are likely due to the fact that significantly fewer layer II/III neurons are labeled in *Thy1*-GCaMP2.2c mice (Figure 1; Figure S2).

We also imaged neuronal activity in the motor cortex of awake mice using a fixed-head imaging design (Dombeck et al., 2007, 2009). In awake, behaving animals, we were able to detect activated neurons both in *Thy1*-GCaMP2.2c and *Thy1*-GCaMP3 mice (Figures 6A and 6B; Figure S6; Movie S7). In *Thy1*-GCaMP3 mice, we detected many more activated neurons (34.4 ± 1.7 cells in a 250 × 250 μm imaging window, n = 5 areas from 3 mice) over a 10 min period (Figures 6A and 6B) compared to anesthetized animals (see above). The population activity in the primary motor cortex of both *Thy1*-GCaMP mice was correlated with locomotor activity (Figure 6C; Figure S6). Repeated imaging of the same brain area at 15 days after the first imaging showed that most of the same neurons were active in both views (Figure 6D). From these observations, we conclude that both *Thy1*-GCaMP2.2c and *Thy1*-GCaMP3 mice can be used to monitor neuronal activity over extended periods of time in the motor cortex of living animals.

In Vivo Imaging of Sensory Stimulation-Evoked Ca^{2+} Transients in the Somatosensory Cortex

In recent studies, viral expression of the ratiometric GECIs (YC3.60 and D3cpV) and GCaMP3 in pyramidal neurons of the mouse somatosensory (barrel) cortex allowed the detection of neuronal activity induced by whisker stimulation (Lütcke et al., 2010; Mittmann et al., 2011; O'Connor et al., 2010; Wallace et al., 2008). To determine whether Ca^{2+} transients could be detected in the barrel cortex in response to sensory stimulation in our *Thy1*-GCaMP mice, we performed a similar test. We used *Thy1*-GCaMP3 mice because in vivo two-photon imaging in the barrel cortex revealed sparse labeling of layer II/III pyramidal neurons in *Thy1*-GCaMP2.2c mice and dense labeling in *Thy1*-GCaMP3 mice (data not shown). To induce sensory stimulation, we deflected multiple mystacial vibrissae ten times using 500 ms air puffs with 10 s interpuff intervals. In *Thy1*-GCaMP3 transgenic mice, we routinely detected calcium transients associated with whisker stimulation in both cell somata and the adjacent layer II/III neuropil (Figures 7A–7C and Movie S8). To further characterize the kinetics of GCaMP3 signals in vivo, we next recorded changes in reporter fluorescence in 64 × 64 pixel frames at a frame rate of 40 Hz from layer II/III GCaMP3-expressing neurons. Single air puffs induced $\Delta F/F$ amplitude changes of 242.9% ± 14.2% (n = 8 from 3 mice), similar to those seen with virally transduced GCaMP3 (O'Connor et al., 2010) and higher than the ratio changes seen from YC 3.60 and D3cpV (Lütcke et al., 2010; Wallace et al., 2008). The rise and decay time of the calcium transients in GCaMP3 were 477.9 ± 17.1 ms and 1,072.5 ± 29.4 ms, respectively (n = 8 from 3 mice; Figures 7D–7F). Thus, *Thy1*-GCaMP3 mice allow the detection of dynamic changes in neuronal activity in vivo in response to sensory stimulation.

In Vivo Ca^{2+} Imaging of Odor Responses in the Olfactory Bulb

In *Thy1*-GCaMP3 transgenic mice, GCaMP is expressed in the glomerular layer, the external plexiform layer, and the mitral cell layer, but not within the olfactory nerve layer or the granule cell layer (Figures S7A and S7B). Two-photon imaging showed that GCaMP3 fluorescence was detected in the olfactory bulb

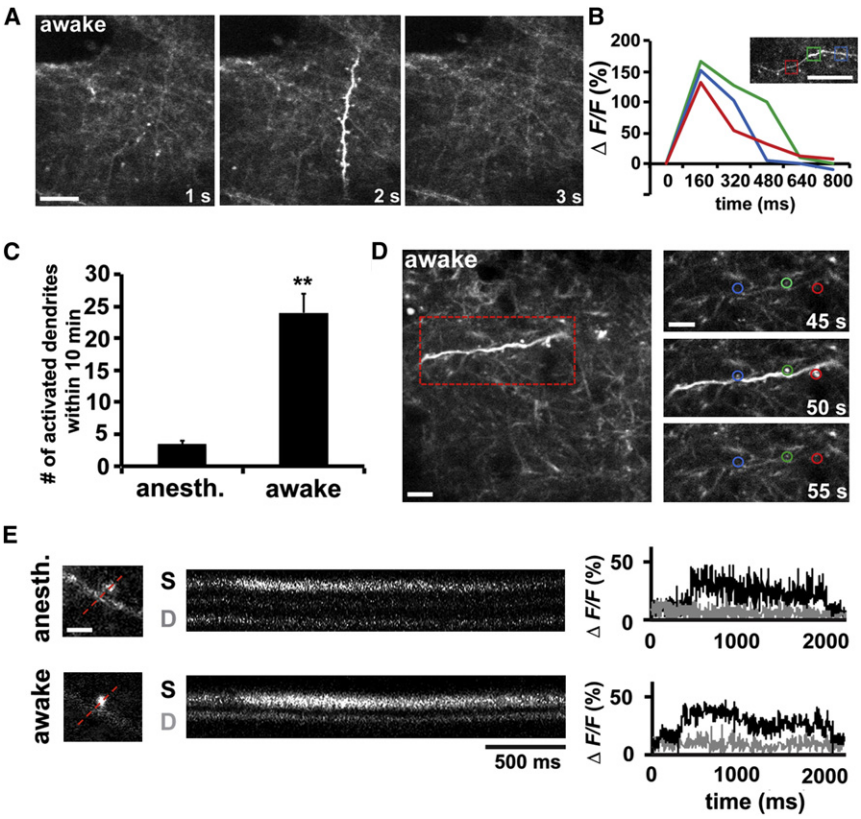

Figure 5. In Vivo Ca^{2+} Imaging of Apical Dendrites and Dendritic Spines of Layer V Pyramidal Neurons in *Thy1*-GCaMP2.2c Transgenic Mice

(A) Two-photon Ca^{2+} imaging of layer V apical dendrites in the motor cortex of an awake, head-fixed *Thy1*-GCaMP2.2c mouse (2 months old). A representative time-lapse sequence shows a dendritic calcium transient in both the dendritic shaft and spines.

(B) A representative $\Delta F/F$ tracing of a dendritic calcium transient within the apical tuft in an awake, head-fixed mouse. Three segments (red, green, and blue boxes) of the dendritic arbor were measured before and after the calcium transient. Note that the calcium transient lasts for hundreds of milliseconds.

(C) Quantification of the number of dendritic calcium transients within 10 min in a 100 × 100 μm imaging window under anesthetized (n = 4 from 3 mice) and awake (n = 6 from 3 mice) state.

(D) Dendritic calcium transient caused a transient calcium elevation in dendritic spines in motor cortex of an awake, behaving mouse. Images of the same apical dendritic segment before (45 s), during (50 s), and after (55 s) its activation are shown. The blue, green, and red circles mark the location of three different spines along the dendrite. See also Movie S6.

(E) A transient calcium elevation could be detected in dendritic spines under anesthetized and awake states. Fluorescence images were acquired from a line scan intersecting a spine (S) and the dendrite (D, gray trace). The increases in fluorescence indicate Ca^{2+} entry within the bulbous spine (black trace).

Data are presented as mean ± SEM. Scale bars represent 10 μm for (A) and (B), 5 μm for (D), and 2 μm for (E). **$p < 0.005$.

in vivo (Figure S7C and Movie S9). Based on the location and soma size, GCaMP3-expressing cells appeared to be mainly mitral cells, in addition to a small subset of periglomerular and external tufted cells. GCaMP fluorescence can be seen throughout the soma and the dendrites.

To characterize activity-induced GCaMP3 responses in the olfactory bulb, we performed in vivo two-photon Ca^{2+} imaging in the dorsal olfactory bulb during odor presentation. For odor stimulation, we chose four odorants, methyl salicylate, amyl acetate, eugenol, and 1-pentanol, because they have different molecular structures and have previously been shown to strongly activate distinct glomeruli in the dorsal olfactory bulb (Lin et al., 2006; Rubin and Katz, 1999; Wachowiak and Cohen, 2001). As shown in Figure S7D, 1% odorants trigger strong calcium responses in the olfactory bulbs of *Thy1*-GCaMP3 mice. Similar to previous in vivo imaging data using Kv3.1 potassium channel promoter-driven expression of GCaMP2.0 in the olfactory bulb (Fletcher et al., 2009), each odor induced two types of signals within the odor maps. The first response type was relatively weak and diffuse, whereas the second type of response was more focused and formed "hot spots" that corresponded to individual glomeruli (Figure S7D). Consistent with previous studies (Wachowiak and Cohen, 2001; Fried et al., 2002; Bozza et al., 2004), we found that different odorants activated discrete glomeruli in *Thy1*-GCaMP3 mice (Figure S7D). We also found that initial odor responses were often higher than subsequent stimuli (Figure S7E), a phenomenon we attributed to odor habituation (Holy et al., 2000; Verhagen et al., 2007). Notably, we found that odorant-triggered fluorescence changes with GCaMP3 are in the range of 30%–150%, much greater than in previous reports that used other calcium indicators (De Saint Jan et al., 2009; Fletcher et al., 2009).

Olfactory coding is multidimensional. In addition to response profiles being dictated by the molecular structure of odorants, odorant concentration also influences the receptor repertoire recruited to the stimulus and thus shapes the composite response pattern. With increasing concentrations of odorants, new glomeruli may be recruited into the response pattern, while previously active glomeruli often respond more intensively (Fletcher et al., 2009; Johnson and Leon, 2000). These effects were observed for all odorants tested in *Thy1*-GCaMP3 mice; the representative odor maps are shown in Figure S7F. Taken together, these data show that *Thy1*-GCaMP3 mice can detect changes of neuronal activity in mitral cells in response to specific odorants in a population and concentration-dependent manner. Furthermore, unlike previous methods for monitoring Ca^{2+}-mediated olfactory responses at presynaptic terminals (Bozza et al., 2004; Fried et al., 2002), the *Thy1*-GCaMP3 reporter line described here reflects postsynaptic responses.

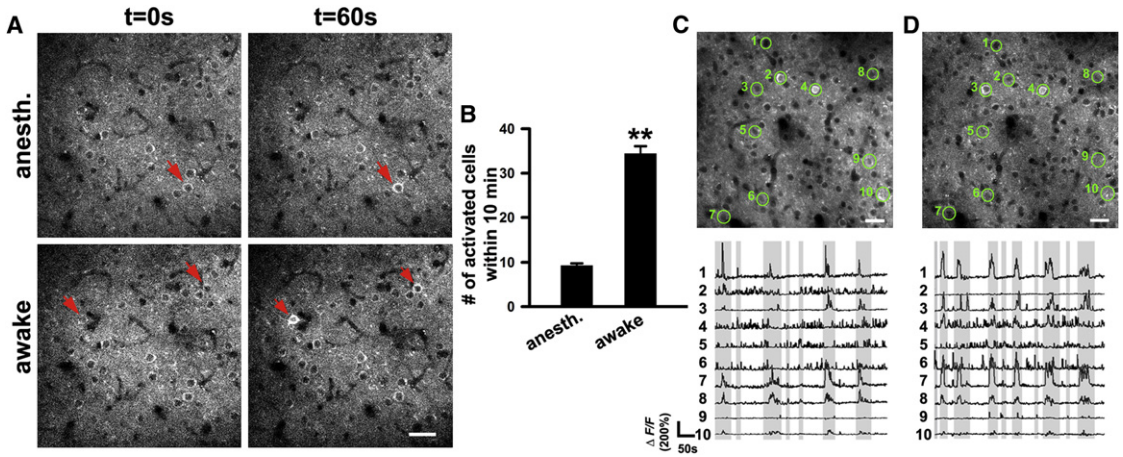

Figure 6. In Vivo Ca^{2+} Imaging of Neuronal Activity in the Motor Cortex with *Thy1*-GCaMP3 Transgenic Mice

(A and B) In vivo two-photon time-lapse images of layer II/III neurons in the motor cortex of 5-month-old *Thy1*-GCaMP3 mice.

(A) Top: examples of neuronal activity in the anesthetized state. Bottom: neuronal activity of the same area in the awake state. Red arrows mark activated neurons.

(B) Quantification of the number of activated neurons within 10 min in anesthetized (n = 4 areas from 3 mice) and awake (n = 5 areas from 3 mice) state. Data are presented as mean ± SEM. **$p < 0.005$.

(C and D) Repeated imaging of calcium dynamics of layer II/III neurons in the motor cortex.

(C) A raw fluorescence image of layer II/III neurons in the motor cortex of *Thy1*-GCaMP3 mice at 7 days after surgery (top) and $\Delta F/F$ traces of each circled neuron (bottom). Shaded part of the traces indicates that the mice were moving.

(D) The fluorescence image of the same field and fluorescent traces of the same neurons as in (C) at 22 days after surgery. Scale bars represent 50 μm for (A), (C), and (D).

DISCUSSION

In this study, we generated transgenic mice that stably express improved GCaMPs, GCaMP2.2c and GCaMP3 (Tian et al., 2009), in subsets of CNS neurons under the control of the mouse *Thy1* promoter. Our findings indicate that these GCaMP transgenic lines provide an excellent tool for detecting neural activity in acute brain slices as well as the intact brain. First, we show that both spontaneous and evoked calcium transients can be detected in acute brain slices prepared from both transgenic lines. Notably, we were able to detect small calcium transients in neuronal somata triggered by a single action potential. Second, calcium transients were also readily detected in apical dendrites and dendritic spines in the living cortex of *Thy1*-GCaMP2.2c transgenic mice. Third, large, robust calcium signals can be detected in populations of layer II/III cortical neurons in both GCaMP transgenic lines with natural motor or sensory stimuli. Lastly, odor-evoked calcium transients can be detected at single glomerulus resolution in *Thy1*-GCaMP3 mice. Together, these results indicate that GCaMP2.2c and GCaMP3 mice provide a sensitive means to detect patterns of neuronal activity at the level of individual neurons and synapses, as well as populations of neurons in vitro and in vivo.

Until recently, calcium imaging with synthetic calcium dyes has been the method of choice to monitor activity in neuronal cultures, acute brain slices, and intact brains. However, routine and reliable loading of Ca^{2+} dyes into targeted neuronal populations in vivo has proven difficult. Bulk loading of calcium indicators indiscriminately labels mixtures of cells, making cell type-specific labeling nearly impossible. Single-cell labeling is technically challenging and allows for only a few cells to be loaded during a given imaging session. Furthermore, imaging with calcium dyes can only last for periods of hours, making chronic recordings of neuronal activity over extended times difficult, if not impossible. Genetically encoded calcium indicators overcome many of these limitations (Hasan et al., 2004; Looger and Griesbeck, 2012; Miyawaki et al., 1997). Incremental rounds of reporter optimization have resulted in new GCaMPs with significantly improved fluorescence characteristics and higher sensitivity to calcium (Muto et al., 2011; Ohkura et al., 2005; Souslova et al., 2007; Tallini et al., 2006; Tian et al., 2009; Zhao et al., 2011b).

A number of methods are available for transgene delivery, including in utero electroporation, biolistic delivery, and viral transduction. Some viral delivery methods have distinct advantages, e.g., the retrograde transsynaptic tracing ability afforded by rabies virus, into which GCaMP3 has recently been incorporated (Osakada et al., 2011). However, they have a number of drawbacks as well: limited payload capacity, inherent tropism, local delivery, incompatibility with early developmental events, and the requirement that each experimental animal be subjected to a survival surgery. Only transgenic incorporation into the genome affords stable expression of a transgene in all target tissues, reliable animal-to-animal comparisons, and the ability to image the embryo and other early developmental states. In this study, we demonstrated the feasibility and functionality of long-term expression of GCaMPs from the *Thy-1* promoter for in vitro and in vivo calcium imaging.

As any GECI buffers Ca^{2+} and may interfere with endogenous signaling events, there is an inherent risk of neuronal toxicity with long-term and/or high levels of expression. Indeed, overexpression of GCaMP3 using in utero electroporation or viral infection

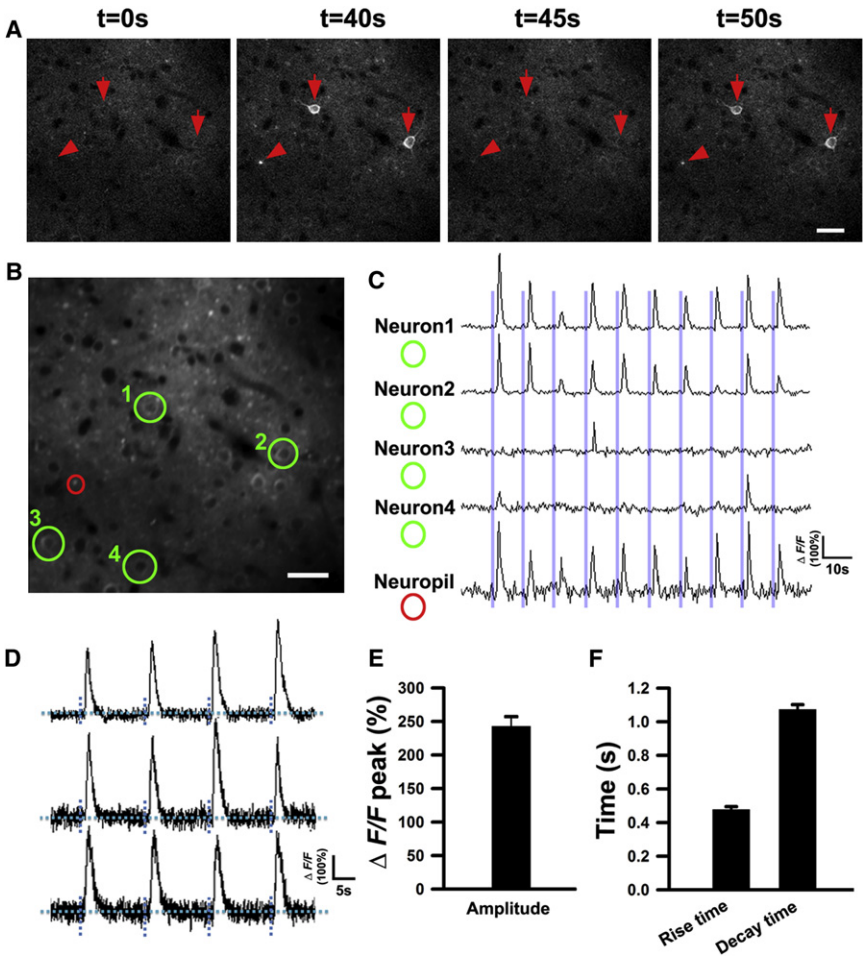

Figure 7. In Vivo Imaging of Sensory Stimulation-Evoked Calcium Transients in the Somatosensory Cortex of *Thy1*-GCaMP3 Transgenic Mice

(A) In vivo two-photon time-lapse images of layer II/III neurons in the somatosensory cortex of *Thy1*-GCaMP3 mice. Red arrows mark activated neurons and a red arrowhead marks an activated neuronal process.

(B and C) Calcium dynamics of layer II/III neurons in the somatosensory cortex. A raw fluorescence image of layer II/III neurons is shown in (B). Fluorescence traces of the neurons (green circles) and neuropil (red circle) are shown in (C). The blue bars show the onset of air puffs. See also Movie S8.

(D) Three examples of individual fluorescence traces of layer II/III neurons in the somatosensory cortex using 40 Hz scanning speed.

(E) The average maximal fluorescence changes in response to a single air puff.

(F) Decay time and rise time of neurons in response to a single air puff.

Data are presented as mean ± SEM (n = 8 cells from 3 mice for E and F). Scale bars represent 50 μm for (A) and (B).

showed that high expression levels can induce neural dysfunction and altered subcellular localization (e.g., nuclear), particularly near the injection site (Dombeck et al., 2010; Tian et al., 2009). In our transgenic animals, GCaMP was widely expressed in many neuronal subtypes throughout the CNS. Analysis of *Thy1*-GCaMP2.2c and *Thy1*-GCaMP3 transgenic mice did not reveal any obvious gross or cellular abnormalities. Importantly, distribution of GCaMP was cytosolic and homogeneous, with no signs of aggregation or compartmentalization in the nucleus in vivo. These results suggest that our transgenic mice exhibit stable, long-term expression of GCaMPs in neurons with normal functions and thus allow sensitive detection of calcium transients in vivo.

One key advantage of calcium imaging is that it allows the simultaneous mapping of neuronal activities from numerous cells within complex neuronal networks. Given that GCaMP3 transgenic expression targets most pyramidal neurons (~90%) throughout the cortical layers, this mouse line could allow activity monitoring from large populations of neurons across various cortical layers in behaving animals. The stable expression of GCaMP3 at nontoxic levels in our transgenic mice makes their application ideal for long-term in vivo monitoring of somatic activity. On the other hand, due to the low basal fluorescence and sparser labeling, *Thy1*-GCaMP2.2c mice provide a suitable means for imaging of Ca^{2+} transients in the dendrites of layer V neurons in vivo. Large calcium transients could readily be detected in dendrites and dendritic spines of layer V pyramidal neurons in *Thy1*-GCaMP2.2c mice and in the somata of layer II/III neurons in *Thy1*-GCaMP3 transgenic mice.

In the CNS, odors are represented as patterns of neural activity encoded by time and space. Previous mapping approaches in the olfactory bulb have used 2-deoxyglucose staining, intrinsic optical signal imaging, and pH-sensitive exocytosis detection to monitor odor-induced changes in neuronal activity. Such functional mapping strategies can provide temporal and spatial resolution of neuronal activity but to date have primarily reported olfactory nerve presynaptic activity, with little (or no) contribution from postsynaptic neurons. On the other hand, odor responses imaged by bulk-loaded voltage-sensitive dyes comprise a mixture of both pre- and postsynaptic components and do not show genetic specificity (Friedrich and Korsching, 1998; Spors and Grinvald, 2002). More recently, GCaMP2.0 transgenic mice, driven by a Kv3.1 potassium channel promoter, allowed detection of postsynaptic odor representation within the glomerular cell layer, but responses were relatively weak and did not span a dynamic range of odor concentration or specificity (Fletcher et al., 2009). In *Thy1*-GCaMP3 mice, GCaMP3 is expressed strongly in the glomerular and mitral cell layers, and responses to odorants were encoded by distinct sets of glomeruli. Concentration coding involved both graded responses from each activated glomerulus, as well as an increase in the total number of

glomeruli that responded. Compared to GCaMP2.0 transgenic mice, baseline expression and odor-induced changes in GCaMP fluorescence was significantly higher in *Thy1*-GCaMP3 mice. These findings suggest that the *Thy1*-GCaMP3 transgenic mouse is an improved genetic tool to investigate neuronal activity changes within the olfactory system.

Although our studies only tested the utility of the *Thy1*-GCaMP mice in the motor cortex, somatosensory cortex, and the olfactory bulb, GCaMP expression in these mice was widespread (Figures 1 and 2; Figures S2 and S3), and the strains are likely to be useful for monitoring neuronal activity in many brain areas. Stable expression of GCaMP via transgenic mice will enhance our ability to study how information is processed in both the healthy and diseased brain. Together with the recently generated Cre-inducible GCaMP3 mice (Zariwala et al., 2012), these tools may provide important insights into disease processes and activity-related pathological changes when combined with animal models of neurological disorders. Furthermore, chronic imaging of various subtypes of neurons with GCaMP will help to pinpoint the important groups of neurons, brain regions, and characteristic abnormalities involved in the onset, progression, and end stages of neurological disorders.

EXPERIMENTAL PROCEDURES

Animal Use

All experiments were conducted according to protocols approved by the Institutional Animal Care and Use and Institutional Biosafety Committees of MIT and the NYU School of Medicine.

DNA Constructs

GCaMP2.0 and GCaMP3 expression constructs were previously reported (Tian et al., 2009). GCaMP2.2c was generated by changing the second arginine to valine and serine at 118 to cysteine of GCaMP2.0. All in vitro expression constructs of GCaMPs were connected with the coding sequence of tdTomato via a 2A peptide (P2A) sequence and subcloned into a modified pBluescript plasmid, which contained the *CAG* promoter (a combination of the cytomegalovirus early enhancer element and chicken beta-actin promoter). To generate the *Thy1*-GCaMP transgenic mouse, we subcloned GCaMP2.2c and GCaMP3 coding sequences into a *Thy1* transgenic construct (Arenkiel et al., 2007; Feng et al., 2000). All constructs were verified by sequencing.

Fluorescence Measurements in HEK293 Cells

HEK293 cells were cultured in DMEM/F12 containing 10% FBS and GCaMP-P2A-tdTomato plasmid transfection was performed with Lipofectamine 2000. Imaging experiments were performed ~36–48 hr after the transfection as described previously (Nakai et al., 2001). Imaging was performed using an Olympus Fluoview 1000 confocal microscope equipped with multiline argon laser (457 nm, 488 nm, and 515 nm) and HeNe (G) laser (543 nm) using the 20× water-immersion objective (NA = 0.5). Green GCaMP fluorescence was excited at 488 nm and isolated using a band-pass filter (505–525 nm). Red tdTomato fluorescence was excited at 543 nm and isolated using a band-pass filter (560–660 nm). The time-series images (XYT) were acquired at frame rates of 1 Hz at a resolution of 256 × 256 pixels. For ATP stimulation, the solution contained 135 mM NaCl, 5.4 mM KCl, 2 mM CaCl2, 1 mM MgCl2, 10 mM glucose, 5 mM HEPES (pH 7.4), and 100 μM ATP. All experiments were performed at room temperature.

Transgenic Mice

Thy1-GCaMP2.2c and *Thy1*-GCaMP3 transgenic mice were generated by injection of gel-purified DNA into fertilized oocytes using standard techniques (Feng et al., 2004; Zhao et al., 2011a). Embryos for injection were obtained by mating (C57BL6/J and CBA) F1 hybrids. Transgenic founders were backcrossed to C57BL6/J mice for analysis of expression patterns. Primers for genotyping were 5′- TCT GAG TGG CAA AGG ACC TTA GG −3′ (forward) 5′- TTA CGA CGT GAT GAG TCG ACC −3′ (reverse). The mouse strains have been deposited at The Jackson Laboratory. The JAX stock number for *Thy1*-GCaMP2.2c line 8 is 017892 and the JAX stock number for *Thy1*-GCaMP3 line 6 is 017893.

Immunohistochemistry

GCaMP mice were anesthetized by the inhalation of isoflurane and were intracardially perfused with 20 ml 1× PBS, followed by 20 ml 4% paraformaldehyde (PFA) in PBS. Mouse brains were then postfixed in 4% PFA/PBS overnight at 4°C. We cut 50 μm sagittal sections using a vibratome. Rabbit anti-GFP antibody (Invitrogen, 1:1,000) was used to enhance the GCaMP fluorescence. Briefly, sections were incubated with blocking buffer (5% normal goat serum, 2% BSA, and 0.2% Triton X-100 in 1× PBS) for 1 hr at room temperature and then incubated with rabbit anti-GFP antibody overnight at 4°C. After incubation with the first antibody, sections were washed with 1× PBS three times for 20 min each, followed by incubation with Alexa 488-conjugated goat anti-rabbit secondary antibody (Invitrogen) for 2–4 hr at room temperature and then washed with 1× PBS. Sections were transferred onto slides, mounted with 0.1% paraphenylinediamine in 90% glycerol/PBS, and imaged with a microscope (BX61, Olympus).

Slice Preparation and Electrophysiology

Acute slices were prepared according to published procedures (Peça et al., 2011). Briefly, mice were anesthetized with Avertin solution (20 mg/ml, 0.5 mg/g body weight) and perfused through the heart with 20 ml of ice-cold oxygenated (95% O_2, 5% CO_2) cutting solution containing 105 mM NMDG, 105 mM HCl, 2.5 mM KCl, 1.2 mM NaH_2PO_4, 26 mM $NaHCO_3$, 25 mM glucose, 10 mM $MgSO_4$, 0.5 mM $CaCl_2$, 5 mM L-ascorbic acid, 3 mM sodium tyruvate, and 2 mM thiourea (pH was 7.4, with osmolarity of 295–305 mOsm). The brains were rapidly removed and placed in ice-cold oxygenated cutting solution. Coronal or transverse hippocampal slices (300 μm) were prepared using a slicer (Vibratome 1000 Plus, Leica Microsystems) and then transferred to an incubation chamber (BSK4, Scientific System Design) at 32°C with carbogenated cutting solution, which was gradually replaced with artificial cerebral spinal fluid (ACSF) in 30 min through a peristaltic pump (Dynamax Model RP-1; Rainin Instruments), allowing a precise regulation of fluid flow rates. The slices were then kept in the ACSF that contained 119 mM NaCl, 2.3 mM KCl, 1.0 mM NaH_2PO_4, 26 mM $NaHCO_3$, 11 mM glucose, 1.3 mM $MgSO_4$, and 2.5 mM $CaCl_2$ (pH was adjusted to 7.4 with HCl, with osmolarity of 295–305 mOsm) at room temperature for at least 30 min.

Recordings were performed in oxygenated ACSF. Intracellular solution consisted of 130 mM $KMeSO_3$, 10 mM HEPES, 4 mM $MgCl_2$, 4 mM Na_2ATP, 0.4 mM NaGTP, 10 mM Na-phosphocreatine, and 3 mM Na-L-ascorbate; pH was adjusted to 7.3 with KOH. Recordings were performed at room temperature in ACSF. To evoke APs, we held cells in the current-clamp configuration, and we injected 3–5 nA of current for 2 ms through the recording electrode. Cells were selected if their GCaMP fluorescence was homogeneously distributed in the cytoplasm.

Fluorescent signals were imaged by a confocal microscope (Fluoview FV 1000; Olympus) with a 30 mW multiline argon laser, at 5%–10% laser power. The laser with a wavelength of 488 nm was used for excitation, and fluorescence was recorded through a band-pass filter (505–525 nm). The images were acquired using 40× water-immersion objectives (NA = 0.8) with 5 Hz scanning speed. XYT image galleries were collected and average fluorescence intensity in the soma was measured for the quantification by Fluoview data processing software. We report time series as $\Delta F/F = [(F - F_B) - (F0 - F_B)]/(F0 - F_B)$, where F is the raw fluorescence signal, F_B is the background, and F0 is the mean fluorescence signal in a baseline period prior to the action potential stimuli. SNR was calculated as the ratio of $\Delta F/F$ to SD of the basal fluorescence, 1 s before the stimulus up to stimulus onset. Rise time was measured as the time between onset of current injection and the maximal response. Decay time was measured as the time between the maximal response and the decay back to baseline.

In Vivo Ca^{2+} Imaging of Layer V Apical Dendrites in Motor Cortex

A head holder composed of two parallel micrometal bars was attached to the animal's skull to reduce motion-induced artifact during imaging. First, surgical anesthesia was achieved with an intraperitoneal injection (5–6 μl/g) of a mixture of ketamine (20 mg/mL) and xylazine (3 mg/mL). A midline incision of the scalp exposed the periosteum, which was manually removed with a microsurgical blade. A small skull region (~0.2 mm in diameter) was located over the left motor cortex based on stereotactic coordinates (0.5 mm posterior from the bregma and 1.5 mm lateral from the midline) and marked with a pencil. A thin layer of cyanoacrylate-based glue was first applied to the top of the entire skull surface and to the metal bars, and the head holder was then further fortified with dental acrylic cement (Lang Dental Manufacturing). The dental cement was applied so that a well was formed leaving the motor cortex with the marked skull region exposed between the two bars. All procedures were performed under a dissection microscope. After the dental cement was completely dry, the head holder was screwed to two metal cubes that were attached to a solid metal base, and a cranial window was created over the previously marked region. The procedures for preparing a thinned skull cranial window for two-photon imaging have been described in detail in previous publications (Yang et al., 2010). Briefly, a high-speed drill was used to carefully reduce the skull thickness by approximately 50% under a dissecting microscope. The skull was immersed in artificial cerebrospinal fluid during drilling. Skull thinning was completed by carefully scraping the cranial surface with a microsurgical blade to ~20 μm in thickness. For anesthetized imaging, animals were immediately imaged under a two-photon microscope tuned to 910 nm with a 40× objective immersed in an artificial cerebrospinal fluid solution and a 3× digital zoom. For awake animal imaging, the completed cranial window was covered with silicon elastomer (World Precision Instruments) and mice were given at least 4 hr to recover from the surgery-related anesthesia. Mice with head mounts were habituated for a few times (10 min for each time) in the imaging apparatus to minimize potential stress effects of head restraining and imaging. To image dendrites in awake mice, we screwed the head holder to two metal cubes attached to a solid metal base, and the silicon elastomer was peeled off to expose the thinned skull region and ACSF was added to the well. The head-restrained animal was then placed on the stage of a two-photon microscope.

These in vivo two-photon imaging experiments were performed using a Bio-Rad Radiance 2000 two-photon system equipped with a Tsunami Ti:sapphire laser pumped by a 10 W MilleniaXs laser (Spectra-Physics). The average laser power on the sample is ~20–30 mW. Most experiments were acquired at frame rates of 1 Hz at a resolution of 512 × 512 pixels using a 40× water-immersion objective (Nikon). Image acquisition was performed using Laser Sharp 2000 software and analyzed post hoc using ImageJ software (NIH). $\Delta F/F$ was calculated identical to slice imaging experiments. For detecting calcium signals in layer V apical tuft dendritic spines, a line crossing the dendrite and the middle of the spine head was drawn and fluorescence intensity along the line was measured using ImageJ (NIH).

In Vivo Ca^{2+} Imaging of Neuronal Activity in the Motor Cortex, Somatosensory Cortex, and Olfactory Bulb

Imaging experiments were performed on 4- to 5-month-old mice. The surgery was performed as described previously (Dombeck et al., 2009). Briefly, the mice were anesthetized with Avertin solution (20 mg/ml, 0.5 mg/g body weight) and were placed in a stereotactic apparatus with a heating pad underneath to maintain body temperature. A 2 × 2 mm piece of bone was removed above the motor cortex, somatosensory cortex, or olfactory bulb as determined by stereotactic coordinates, and the dura was kept intact and moist with saline. To dampen heartbeat and breathing-induced motion, we filled the cranial window with Kwik-sil (World Precision Instruments) and covered it with an immobilized glass coverslip. A custom-designed head plate was cemented on the cranial window with Meta-bond (Parkell) when the Kwik-sil set. For chronic imaging, two coverslips were joined with ultraviolet curable optical glue (NOR-138, Norland). A smaller insert fit into the craniotomy and a larger piece was attached to the bone. Imaging was performed 7 days postsurgery to allow the window to clear.

During imaging of neuronal activity in motor cortex, the head-fixed animals were placed in water to induce swimming-like behavior. The animals were kept alert by presenting a pole or by mild air puffs to the whisker field. An infrared charge-coupled device camera (CCTV) was used for observing the animal's behavior during imaging sessions.

Sensory stimulations, consisting of puffs of compressed air delivered by a Picospritzer unit (Picospritzer II; General Valve), were applied through a 1-mm-diameter glass pipette placed 15–25 mm rostrolateral from the whiskers. Air puffs (500 ms duration) were given ten times with 10 s intervals to prevent adaptation of whisker-evoked responses.

Odorants were delivered using a custom-built odor delivery system in which the saturated vapor of an odorant was diluted into a main stream of clean air. The clean air stream was fixed at 0.6–0.8 L/min throughout the experiment and the odor vapor stream was adjusted to give the final concentration to the animal. A tube opening was positioned <1 cm from the animal's nostrils. To avoid cross-contamination, we used separate Teflon tubing in parallel for delivery of different odorants. Odorants were usually presented with pulse duration of 1 s and interstimulus interval of 30 s to avoid potential sensory adaptation. A constant suction system was positioned close to the odorant delivery system and used to quickly remove remnant odorants. The odorants used in this study included methyl salicylate, amyl acetate, eugenol, and 1-pentanol (Sigma-Aldrich).

In these experiments, in vivo two-photon imaging was performed at the McGovern Institute two-photon microscopy core facility. Imaging was performed on a custom two-photon laser-scanning microscope (Ultima; Prairie Technologies) coupled with a Mai Tai Deep See laser (Spectra Physics). The laser was operated at 910 nm (~30–40 mW average power on the sample). The emission filter set for imaging GCaMP fluorescence consisted of a 575 nm dichroic mirror and a 525/70 nm band-pass filter. Fluorescence signal was detected using Hamamatsu multialkali PMTs. In most experiments, images were acquired at frame rates of 1.5–2 Hz at a resolution of 512 × 256 pixels using a 20×, 1.0 NA water-immersion objective (Zeiss). For in vivo z stack imaging, images were taken at a resolution of 512 × 512 pixels with 2 μm intervals. Image acquisition was performed using custom Prairie View Software. The images were analyzed post hoc using NIH ImageJ and Image-Pro Plus 5.0 software (Media Cybernetics). $\Delta F/F$ was calculated identical to slice imaging experiments.

Statistical Analysis

All statistical analyses were performed using SPSS (IBM) software and graphs were drawn in SigmaPlot 2000 (Systat Software). Values are expressed as mean ± SEM. The data between two groups were compared using unpaired t test. The data among three groups were compared using one-way ANOVA. Statistical significance was defined as $^*p < 0.05$ or $^{**}p < 0.005$.

SUPPLEMENTAL INFORMATION

Supplemental Information includes seven figures and nine movies and can be found with this article online at http://dx.doi.org/10.1016/j.neuron.2012.07.011.

ACKNOWLEDGMENTS

We thank the members of the Feng laboratory for helpful discussions. We would like to give special thanks to Peimin Qi, Ethan Skowronski-Lutz, Tyler Clark Brown, Mriganka Sur, Caroline Runyan, and Holly Robertson for their intellectual input and technical help. We also thank Charles Jennings and Thomas J. Diefenbach in the McGovern Institute two-photon microscopy core facility for their technical support. This work was made possible by the support from an anonymous grant and from The Poitras Center for Affective Disorders Research to G.F, by National Institutes of Health Grant NS047325 to W.-B.G, and by The McNair Foundation and NINDS R00NS64171 and NIH grant R01NS078294 to B.R.A.

Accepted: July 3, 2012
Published: October 17, 2012

REFERENCES

Andermann, M.L., Kerlin, A.M., Roumis, D.K., Glickfeld, L.L., and Reid, R.C. (2011). Functional specialization of mouse higher visual cortical areas. Neuron *72*, 1025–1039.

Arenkiel, B.R., Peca, J., Davison, I.G., Feliciano, C., Deisseroth, K., Augustine, G.J., Ehlers, M.D., and Feng, G. (2007). In vivo light-induced activation of neural circuitry in transgenic mice expressing channelrhodopsin-2. Neuron *54*, 205–218.

Borghuis, B.G., Tian, L., Xu, Y., Nikonov, S.S., Vardi, N., Zemelman, B.V., and Looger, L.L. (2011). Imaging light responses of targeted neuron populations in the rodent retina. J. Neurosci. *31*, 2855–2867.

Bozza, T., McGann, J.P., Mombaerts, P., and Wachowiak, M. (2004). In vivo imaging of neuronal activity by targeted expression of a genetically encoded probe in the mouse. Neuron *42*, 9–21.

Chen, X., Leischner, U., Rochefort, N.L., Nelken, I., and Konnerth, A. (2011). Functional mapping of single spines in cortical neurons in vivo. Nature *475*, 501–505.

De Saint Jan, D., Hirnet, D., Westbrook, G.L., and Charpak, S. (2009). External tufted cells drive the output of olfactory bulb glomeruli. J. Neurosci. *29*, 2043–2052.

Dombeck, D.A., Khabbaz, A.N., Collman, F., Adelman, T.L., and Tank, D.W. (2007). Imaging large-scale neural activity with cellular resolution in awake, mobile mice. Neuron *56*, 43–57.

Dombeck, D.A., Graziano, M.S., and Tank, D.W. (2009). Functional clustering of neurons in motor cortex determined by cellular resolution imaging in awake behaving mice. J. Neurosci. *29*, 13751–13760.

Dombeck, D.A., Harvey, C.D., Tian, L., Looger, L.L., and Tank, D.W. (2010). Functional imaging of hippocampal place cells at cellular resolution during virtual navigation. Nat. Neurosci. *13*, 1433–1440.

Feng, G., Mellor, R.H., Bernstein, M., Keller-Peck, C., Nguyen, Q.T., Wallace, M., Nerbonne, J.M., Lichtman, J.W., and Sanes, J.R. (2000). Imaging neuronal subsets in transgenic mice expressing multiple spectral variants of GFP. Neuron *28*, 41–51.

Feng, G., Lu, J., and Gross, J. (2004). Generation of transgenic mice. Methods Mol. Med. *99*, 255–267.

Fletcher, M.L., Masurkar, A.V., Xing, J., Imamura, F., Xiong, W., Nagayama, S., Mutoh, H., Greer, C.A., Knöpfel, T., and Chen, W.R. (2009). Optical imaging of postsynaptic odor representation in the glomerular layer of the mouse olfactory bulb. J. Neurophysiol. *102*, 817–830.

Fried, H.U., Fuss, S.H., and Korsching, S.I. (2002). Selective imaging of presynaptic activity in the mouse olfactory bulb shows concentration and structure dependence of odor responses in identified glomeruli. Proc. Natl. Acad. Sci. USA *99*, 3222–3227.

Friedrich, R.W., and Korsching, S.I. (1998). Chemotopic, combinatorial, and noncombinatorial odorant representations in the olfactory bulb revealed using a voltage-sensitive axon tracer. J. Neurosci. *18*, 9977–9988.

Hasan, M.T., Friedrich, R.W., Euler, T., Larkum, M.E., Giese, G., Both, M., Duebel, J., Waters, J., Bujard, H., Griesbeck, O., et al. (2004). Functional fluorescent Ca2+ indicator proteins in transgenic mice under TET control. PLoS Biol. *2*, e163.

Hendel, T., Mank, M., Schnell, B., Griesbeck, O., Borst, A., and Reiff, D.F. (2008). Fluorescence changes of genetic calcium indicators and OGB-1 correlated with neural activity and calcium in vivo and in vitro. J. Neurosci. *28*, 7399–7411.

Holy, T.E., Dulac, C., and Meister, M. (2000). Responses of vomeronasal neurons to natural stimuli. Science *289*, 1569–1572.

Johnson, B.A., and Leon, M. (2000). Modular representations of odorants in the glomerular layer of the rat olfactory bulb and the effects of stimulus concentration. J. Comp. Neurol. *422*, 496–509.

Kerr, J.N., and Denk, W. (2008). Imaging in vivo: watching the brain in action. Nat. Rev. Neurosci. *9*, 195–205.

Larkum, M.E., Nevian, T., Sandler, M., Polsky, A., and Schiller, J. (2009). Synaptic integration in tuft dendrites of layer 5 pyramidal neurons: a new unifying principle. Science *325*, 756–760.

Lin, Y., Shea, S.D., and Katz, L.C. (2006). Representation of natural stimuli in the rodent main olfactory bulb. Neuron *50*, 937–949.

Looger, L.L., and Griesbeck, O. (2012). Genetically encoded neural activity indicators. Curr. Opin. Neurobiol. *22*, 18–23.

Lütcke, H., Murayama, M., Hahn, T., Margolis, D.J., Astori, S., Zum Alten Borgloh, S.M., Göbel, W., Yang, Y., Tang, W., Kügler, S., et al. (2010). Optical recording of neuronal activity with a genetically-encoded calcium indicator in anesthetized and freely moving mice. Front Neural Circuits *4*, 9.

Mao, T., O'Connor, D.H., Scheuss, V., Nakai, J., and Svoboda, K. (2008). Characterization and subcellular targeting of GCaMP-type genetically-encoded calcium indicators. PLoS ONE *3*, e1796.

Marshel, J.H., Garrett, M.E., Nauhaus, I., and Callaway, E.M. (2011). Functional specialization of seven mouse visual cortical areas. Neuron *72*, 1040–1054.

Mittmann, W., Wallace, D.J., Czubayko, U., Herb, J.T., Schaefer, A.T., Looger, L.L., Denk, W., and Kerr, J.N. (2011). Two-photon calcium imaging of evoked activity from L5 somatosensory neurons in vivo. Nat. Neurosci. *14*, 1089–1093.

Miyawaki, A., Llopis, J., Heim, R., McCaffery, J.M., Adams, J.A., Ikura, M., and Tsien, R.Y. (1997). Fluorescent indicators for Ca2+ based on green fluorescent proteins and calmodulin. Nature *388*, 882–887.

Muto, A., Ohkura, M., Kotani, T., Higashijima, S., Nakai, J., and Kawakami, K. (2011). Genetic visualization with an improved GCaMP calcium indicator reveals spatiotemporal activation of the spinal motor neurons in zebrafish. Proc. Natl. Acad. Sci. USA *108*, 5425–5430.

Nakai, J., Ohkura, M., and Imoto, K. (2001). A high signal-to-noise Ca(2+) probe composed of a single green fluorescent protein. Nat. Biotechnol. *19*, 137–141.

O'Connor, D.H., Peron, S.P., Huber, D., and Svoboda, K. (2010). Neural activity in barrel cortex underlying vibrissa-based object localization in mice. Neuron *67*, 1048–1061.

Ohkura, M., Matsuzaki, M., Kasai, H., Imoto, K., and Nakai, J. (2005). Genetically encoded bright Ca2+ probe applicable for dynamic Ca2+ imaging of dendritic spines. Anal. Chem. *77*, 5861–5869.

Osakada, F., Mori, T., Cetin, A.H., Marshel, J.H., Virgen, B., and Callaway, E.M. (2011). New rabies virus variants for monitoring and manipulating activity and gene expression in defined neural circuits. Neuron *71*, 617–631.

Peça, J., Feliciano, C., Ting, J.T., Wang, W., Wells, M.F., Venkatraman, T.N., Lascola, C.D., Fu, Z., and Feng, G. (2011). Shank3 mutant mice display autistic-like behaviours and striatal dysfunction. Nature *472*, 437–442.

Pologruto, T.A., Yasuda, R., and Svoboda, K. (2004). Monitoring neural activity and [Ca2+] with genetically encoded Ca2+ indicators. J. Neurosci. *24*, 9572–9579.

Reiff, D.F., Ihring, A., Guerrero, G., Isacoff, E.Y., Joesch, M., Nakai, J., and Borst, A. (2005). In vivo performance of genetically encoded indicators of neural activity in flies. J. Neurosci. *25*, 4766–4778.

Rothschild, G., Nelken, I., and Mizrahi, A. (2010). Functional organization and population dynamics in the mouse primary auditory cortex. Nat. Neurosci. *13*, 353–360.

Rubin, B.D., and Katz, L.C. (1999). Optical imaging of odorant representations in the mammalian olfactory bulb. Neuron *23*, 499–511.

Souslova, E.A., Belousov, V.V., Lock, J.G., Strömblad, S., Kasparov, S., Bolshakov, A.P., Pinelis, V.G., Labas, Y.A., Lukyanov, S., Mayr, L.M., and Chudakov, D.M. (2007). Single fluorescent protein-based Ca2+ sensors with increased dynamic range. BMC Biotechnol. *7*, 37.

Spors, H., and Grinvald, A. (2002). Spatio-temporal dynamics of odor representations in the mammalian olfactory bulb. Neuron *34*, 301–315.

Szymczak, A.L., Workman, C.J., Wang, Y., Vignali, K.M., Dilioglou, S., Vanin, E.F., and Vignali, D.A. (2004). Correction of multi-gene deficiency in vivo using

a single 'self-cleaving' 2A peptide-based retroviral vector. Nat. Biotechnol. *22*, 589–594.

Tallini, Y.N., Ohkura, M., Choi, B.R., Ji, G., Imoto, K., Doran, R., Lee, J., Plan, P., Wilson, J., Xin, H.B., et al. (2006). Imaging cellular signals in the heart in vivo: Cardiac expression of the high-signal Ca2+ indicator GCaMP2. Proc. Natl. Acad. Sci. USA *103*, 4753–4758.

Tian, L., Hires, S.A., Mao, T., Huber, D., Chiappe, M.E., Chalasani, S.H., Petreanu, L., Akerboom, J., McKinney, S.A., Schreiter, E.R., et al. (2009). Imaging neural activity in worms, flies and mice with improved GCaMP calcium indicators. Nat. Methods *6*, 875–881.

Varshavsky, A. (2011). The N-end rule pathway and regulation by proteolysis. Protein Sci. Published online June 1, 2011. http://dx.doi.org/10.1002/pro.666.

Verhagen, J.V., Wesson, D.W., Netoff, T.I., White, J.A., and Wachowiak, M. (2007). Sniffing controls an adaptive filter of sensory input to the olfactory bulb. Nat. Neurosci. *10*, 631–639.

Wachowiak, M., and Cohen, L.B. (2001). Representation of odorants by receptor neuron input to the mouse olfactory bulb. Neuron *32*, 723–735.

Wallace, D.J., Meyer zum Alten Borgloh, S., Astori, S., Yang, Y., Bausen, M., Kügler, S., Palmer, A.E., Tsien, R.Y., Sprengel, R., Kerr, J.N., et al. (2008). Single-spike detection in vitro and in vivo with a genetic Ca2+ sensor. Nat. Methods *5*, 797–804.

Warp, E., Agarwal, G., Wyart, C., Friedmann, D., Oldfield, C.S., Conner, A., Del Bene, F., Arrenberg, A.B., Baier, H., and Isacoff, E.Y. (2012). Emergence of patterned activity in the developing zebrafish spinal cord. Curr. Biol. *22*, 93–102.

Yamada, Y., Michikawa, T., Hashimoto, M., Horikawa, K., Nagai, T., Miyawaki, A., Häusser, M., and Mikoshiba, K. (2011). Quantitative comparison of genetically encoded Ca indicators in cortical pyramidal cells and cerebellar Purkinje cells. Front Cell Neurosci. *5*, 18.

Yang, G., Pan, F., Parkhurst, C.N., Grutzendler, J., and Gan, W.B. (2010). Thinned-skull cranial window technique for long-term imaging of the cortex in live mice. Nat. Protoc. *5*, 201–208.

Yasuda, R., Nimchinsky, E.A., Scheuss, V., Pologruto, T.A., Oertner, T.G., Sabatini, B.L., and Svoboda, K. (2004). Imaging calcium concentration dynamics in small neuronal compartments. Sci. STKE *2004*, pl5.

Young, P., Qiu, L., Wang, D., Zhao, S., Gross, J., and Feng, G. (2008). Single-neuron labeling with inducible Cre-mediated knockout in transgenic mice. Nat. Neurosci. *11*, 721–728.

Zariwala, H.A., Borghuis, B.G., Hoogland, T.M., Madisen, L., Tian, L., De Zeeuw, C.I., Zeng, H., Looger, L.L., Svoboda, K., and Chen, T.W. (2012). A Cre-dependent GCaMP3 reporter mouse for neuronal imaging in vivo. J. Neurosci. *32*, 3131–3141.

Zhao, S., Ting, J.T., Atallah, H.E., Qiu, L., Tan, J., Gloss, B., Augustine, G.J., Deisseroth, K., Luo, M., Graybiel, A.M., and Feng, G. (2011a). Cell type–specific channelrhodopsin-2 transgenic mice for optogenetic dissection of neural circuitry function. Nat. Methods *8*, 745–752.

Zhao, Y., Araki, S., Wu, J., Teramoto, T., Chang, Y.F., Nakano, M., Abdelfattah, A.S., Fujiwara, M., Ishihara, T., Nagai, T., and Campbell, R.E. (2011b). An expanded palette of genetically encoded Ca^{2+} indicators. Science *333*, 1888–1891.